2

[redacted]

NASA-CR-124474) DESIGN AND MATHEMATICAL ANALYSIS OF A THREE-MIRROR X-RAY TELESCOPE BASED ON ATM S-056 X-RAY TELESCOPE HARDWARE Final (Montevallo Univ., Ala.) 60 p HC $5.00 CSCL 20F

N74-12186

Unclas

G3/14 15456

UNIVERSITY OF MONTEVALLO

Design and Mathematical Analysis of a Three-Mirror X-Ray Telescope Based on ATM S-056 X-Ray Telescope Hardware

FINAL REPORT

by

J. William Foreman, Jr.

Joseph M. Cardone

July, 1973

Submitted to

National Aeronautics and Space Administration
George C. Marshall Space Flight Center
Huntsville, Alabama

by

UNIVERSITY OF MONTEVALLO
Montevallo, Alabama

Contract No. NAS8-27301

TABLE OF CONTENTS

I. INTRODUCTION

The basic principles of the three-mirror x-ray telescope (TMXRT) have been described in a previous report[1]. This previous report contains one error, however, which should be rectified at once. In Ref. 1, it was erroneously stated that the P-H channel of the TMXRT forms an inverted image of an x-ray source at infinity, while the H-A channel forms an erect image of the same source. It is true that the P-H channel forms an inverted image, but the fact is that the H-A channel also forms an inverted image. Thus, the images of an off-axis x-ray source at infinity formed by both channels will be on the same side of the optical axis, and not on opposite sides as reported in Ref. 1. The description of the dual-channel mode of operation given in Ref. 1 is therefore inaccurate. With both images on the same side of the optical axis, dual-channel operation is only desirable if both channels have nearly identical effective focal lengths, and form a composite image with reasonable resolution. Fortunately, such a mode of operation is possible, and will be discussed in Section V below.

In this final report the mathematical design of the aspheric third mirror for the TMXRT will be presented, along with the imaging characteristics of the telescope obtained by a ray trace analysis. The present design effort has been directed entirely toward obtaining an aspheric third mirror which will be compatible with existing S-056 paraboloidal-hyperboloidal mirrors. This compatability will facilitate the construction of a prototype model of the TMXRT, since it will only be necessary to fabricate one new mirror in order to obtain a working model.

In designing the aspheric mirror, attention has been concentrated on the fact that the TMXRT is intended for use in cosmic x-ray astronomy (as

opposed to the S-056 telescope, which will be used exclusively for solar x-ray observations). Thus, only a relatively small field of view will be needed in the TMXRT. Furthermore, since the x-ray flux from cosmic x-ray sources is much smaller than that available from the sun, photographic film such as that used in the S-056 telescope is impractical for use in the TMXRT. Cosmic x-ray telescopes will probably make use of arrays of position-sensitive proportional counters for image detection. Since each counter cell has a finite size (typically 1 x 4 millimeters), the resolution requirements on the TMXRT will not be as stringent as those on solar x-ray telescopes.

The work reported herein has been carried out by two faculty members of the Department of Mathematics and Physics at the University of Montevallo: Dr. J. William Foreman, Jr., Professor of Physics (Principal Investigator), and Mr. Joseph M. Cardone, Associate Professor of Mathematics. Work on this project was begun in June, 1971 by Dr. Foreman. Mr. Cardone joined the program in June, 1972. Except for automatic plotting of spot diagrams, all computer programs were run on an XDS-Sigma 5 computer in Wing C of the Astrionics Laboratory at NASA-MSFC. Spot diagrams were plotted (using punched card input data from the Sigma 5) by a Calcomp Model 566 digital plotter controlled by an IBM-1130 computer located in Wing B of the Astrionics Laboratory.

II. SELECTION OF ASPHERIC MIRROR LOCATION AND SIZE

The first step in designing the aspheric third mirror is to choose the approximate location of the mirror along the optical axis. This choice, in turn, determines the physical size of the mirror. The situation is illustrated in Fig. 1. A collimated bundle of rays entering the TMXRT parallel to the optical axis and striking the S-056 hyperboloidal mirror will be brought to a rough focus at a certain point z_{HPF} on the optical axis. This point may be called the hyperboloid pseudo-focus (HPF). A true point focus is not produced, because a hyperboloid exhibits spherical aberration for a point source at infinity. Rays reflected from the hyperboloidal mirror will strike the optical axis at points ranging from z_1 (for rays striking the hyperboloid at its minimum radius, ρ_{HMIN}) to z_2 (for rays which strike the outermost zone of the hyperboloid at radius ρ_{HMAX}). The HPF, which is the location of the circle of least confusion, would be expected to lie halfway between z_1 and z_2. The function of the aspheric third mirror is to intercept the cone of rays leaving the hyperboloidal mirror and produce a point focus at z_{F_2}, as shown in Fig. 1.

In order to determine z_1, z_2, and z_{HPF}, rays were traced using the ray trace equations developed earlier for the S-056 telescope[2]. For an incoming ray parallel to the optical axis which strikes the hyperboloidal mirror at the radius $\rho_{HMIN} = 4.5766776$ inches, the intersection with the optical axis occurs at $z_1 = 98.043$ inches. For an incoming ray at the radius $\rho_{HMAX} = 4.79289648$ inches, the optical axis intersection occurs at $z_2 = 100.034$ inches. (Note: The origin of the coordinate system, as in Ref. 1, lies at the focus of the S-056 paraboloidal mirror. The focal point of the telescope is located at $z_{F_2} = 75.0$ inches.) The longitudinal spread

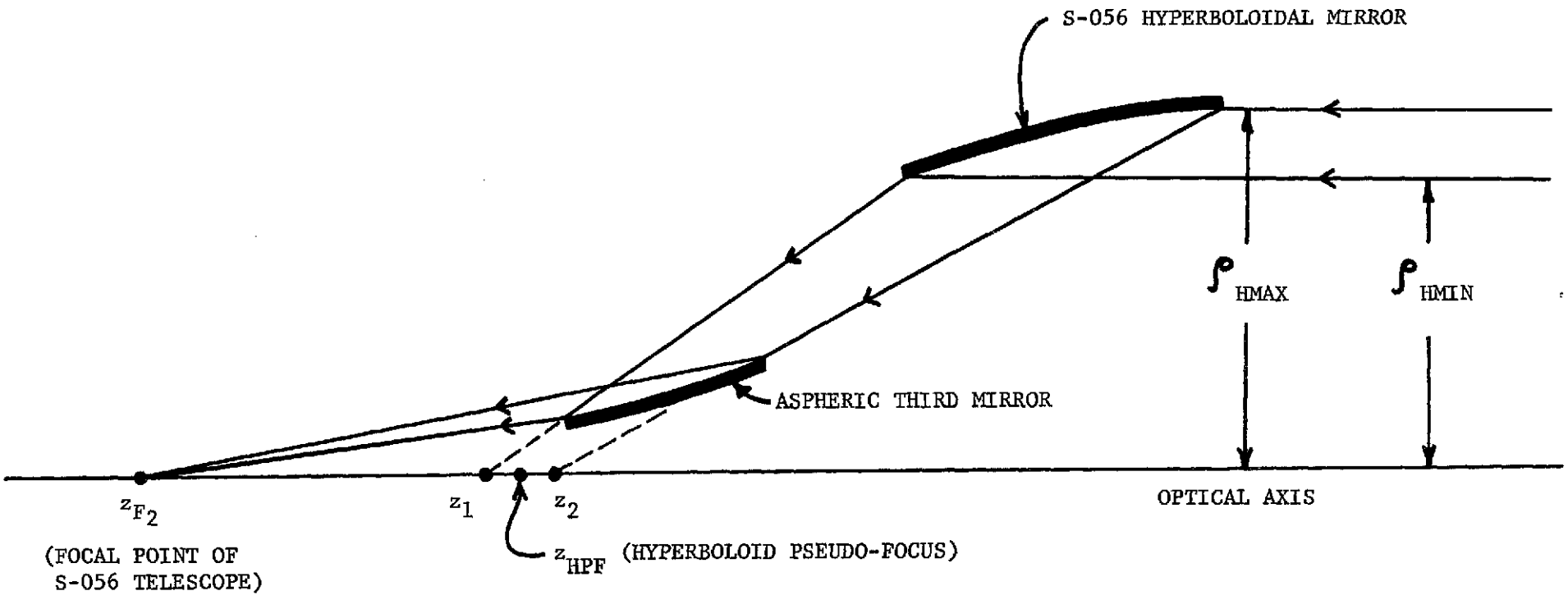

Figure 1. Layout of the optical system of the hyperboloid-aspheric (H-A) channel of the three-mirror x-ray telescope.

along the optical axis is roughly two inches. The HPF should be located midway between z_1 and z_2, at z_{HPF} = 99.039 inches. To check this result, 101 rays were traced through the system (equally spaced from ρ_{HMIN} to ρ_{HMAX}), and the rms diameter of the resulting spot was computed in 11 equally spaced planes from z_1 to z_2, the plane z = 99.039 inches being the central plane. The spot diameter was found to be a minimum in the plane $z = z_{HPF}$ = 99.039 inches, thus confirming the earlier result. The rms spot diameter in the plane $z = z_{HPF}$ is 0.112 inch (2.84 mm).

It was originally thought that the aspheric third mirror would be convex. If this were the case, a hyperboloid of revolution about the optical axis might furnish a good first approximation to the aspheric mirror. With this idea in mind, the first estimate of the aspheric mirror location and size was made by using a hyperboloidal shape for the mirror. To estimate the mean radius of the aspheric mirror, the central ray was chosen from the set of 101 rays used earlier to determine z_{HPF}, and its intersection with various hyperboloidal approximations to the aspheric mirror was found. After reflection from the S-056 hyperboloidal mirror, this ray makes an angle of 5.5° with the optical axis, and intersects the optical axis at z_{OP} = 99.036 inches.

In order for a hyperboloidal approximation to the aspheric third mirror to reflect the particular ray selected above exactly through the focal point z_{F_2} of the S-056 telescope, the focus of the sheet of the hyperboloid which constitutes the mirror itself must lie at the point z_{OP}, and the focus of the other sheet (not physically present) must lie at z_{F_2} (see Fig. 2). The equation of a general hyperboloid with this property is

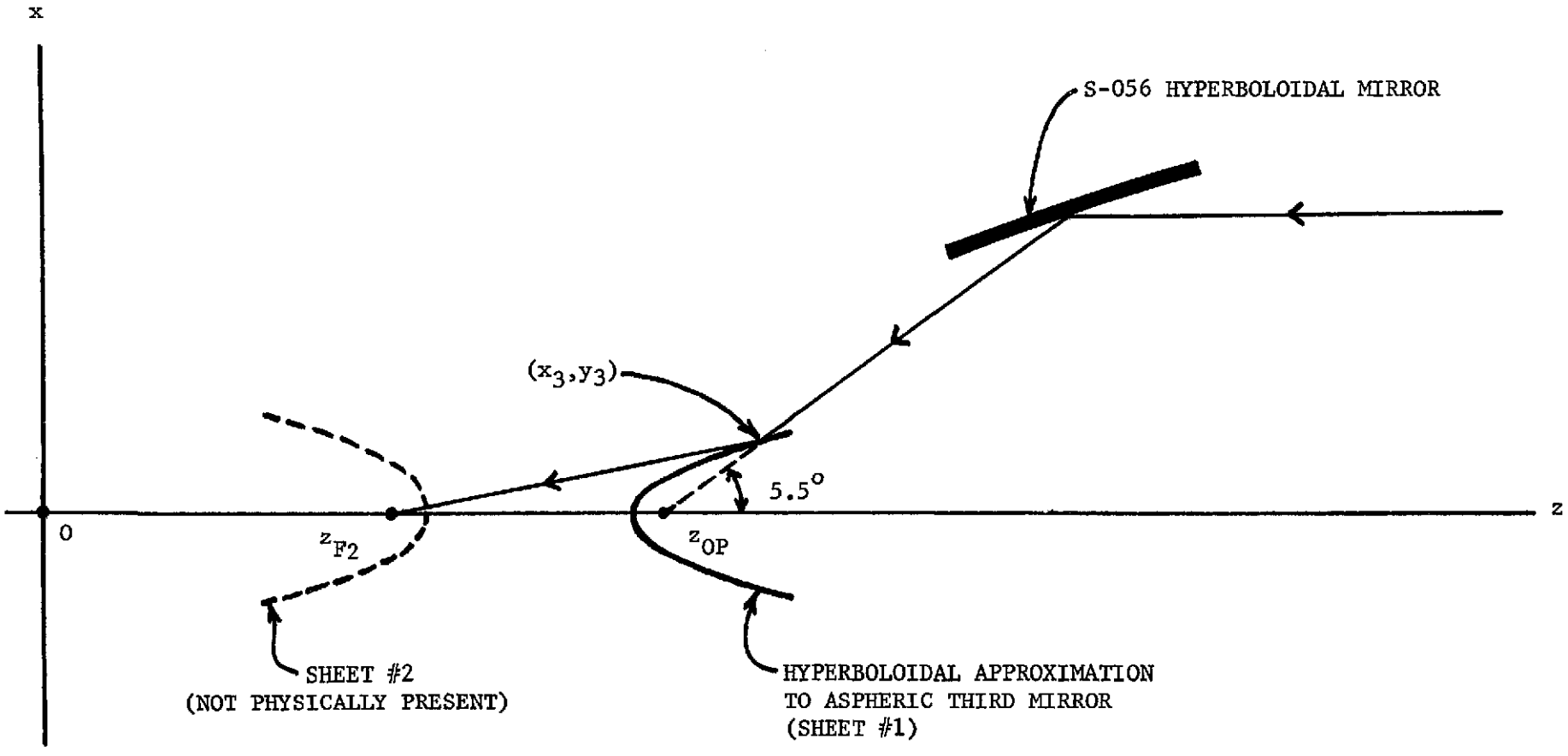

Figure 2. Use of a hyperboloidal approximation to represent the aspheric third mirror.

$$\frac{(z - z_{F_2} - \gamma)^2}{\alpha^2} - \frac{\rho^2}{\beta^2} = 1 \qquad (1)$$

where

$$\gamma = \frac{z_{OP} - z_{F_2}}{2} = 12.018 \text{ inches}$$

$$\rho^2 = x^2 + y^2$$

and

$$\alpha^2 + \beta^2 = \gamma^2 .$$

In addition, in order for the ray to be reflected from the <u>exterior</u> surface of the hyperboloid, the slope of the hyperboloid at the point of intersection with the ray must be less than the slope of the ray. Provided the z-coordinate of the intersection point is not too close to z_{OP}, the slope of the hyperboloid will be nearly equal to the slope of its asymptote,

$$m_A = \frac{\beta}{\alpha} \quad . \tag{2}$$

Since the ray in question makes an angle of 5.5° with the optical axis, an external reflection from the hyperboloid will occur if

$$m_A < \tan 5.5^\circ \quad (= 0.0963). \tag{3}$$

Various hyperboloids of the form of Eq. (1), subject to Eq. (3), can be used to approximate the aspheric third mirror for purposes of estimating its size as a function of location along the optical axis. Table I summarizes the results for various choices of m_A. The coordinates x_3 and z_3 listed in Table I are the coordinates of the point of intersection of the central ray with the hyperboloid in the xz-plane. Thus x_3 represents the nominal mirror radius, and z_3 represents the approximate location of the central segment of the mirror along the optical axis. It was decided in consultation with cognizant NASA-MSFC personnel that a nominal aspheric mirror radius ranging from 1 inch to 2 inches would be acceptable. Attention was therefore concentrated on the middle three cases in Table I.

The final step, still using a hyperboloidal approximation for the aspheric mirror, was to estimate the length of the mirror for the three cases selected

Table I. Coordinates (x_3, z_3) of the point of intersection of the central ray in the xz-plane with various hyperboloids corresponding to different choices of m_A.

m_A	x_3 (inches)	z_3 (inches)
tan 2.5 ° = 0.04366	0.6	105.2
tan 3.0 ° = 0.05421	1.1	110.1
tan 3.5 ° = 0.06116	1.6	115.2
tan 3.75° = 0.06554	2.0	119.7
tan 4.0 ° = 0.06993	2.6	125.7

from Table I. This was done by calculating the z-coordinate of the point of intersection of each hyperboloid with two extreme rays, one striking the S-056 hyperboloidal mirror at a radius of ρ_{HMIN} and the other at a radius of ρ_{HMAX}. The glancing angle of incidence at which the central ray strikes each hyperboloid was also computed to obtain an estimate of the average glancing angle of incidence at each mirror. The results are summarized in Table II.

After further consultation with NASA-MSFC personnel at this stage of the design program, it was decided that the choice $m_A = \tan 3.0°$, which would result in an aspheric third mirror with a nominal diameter of 2 inches and a length of approximately 6 inches, would be the best practical choice. Consequently, all further effort was directed toward designing a mirror which would meet these nominal specifications.

Table II. Complete aspheric mirror parameters as a function of m_A.

m_A	Nominal Mirror Diameter (inches)	Mirror Length (inches)	Glancing Angle of Incidence (degrees)
tan 3°	2.2	6.1	1.87
tan 3.5°	3.2	7.0	1.64
tan 3.75°	4.0	7.8	1.48

III. MIRROR DESIGN FOR ELIMINATION OF SPHERICAL ABERRATION

Design Procedure

Since the TMXRT is intended for observation of cosmic x-ray sources, a large field of view is not required. If an extended cosmic x-ray source is to be examined, the TMXRT can always be operated in a scanning mode. However, it is essential that the on-axis resolution of the TMXRT be as good as possible. The initial aspheric third mirror design was therefore directed entirely toward elimination of spherical aberration in the H-A channel, without attempting to control off-axis performance. An H-A channel free from spherical aberration would at least produce sharp images in the immediate vicinity of the optical axis.

In order to eliminate spherical aberration, it is sufficient to constrain the optical path lengths for rays emanating from an on-axis point source at infinity to be equal as the rays traverse the optical system[3]. In the case of the TMXRT, this constraint can be implemented as follows.

(1) Consider an incoming ray parallel to the optical axis at a distance ρ_{HMIN} from the optical axis. Compute the z-coordinate z_{OP} at which this ray intersects the optical axis after reflection from the S-056 hyperboloidal mirror (see Fig. 3).

(2) Determine the parameters α, β, and γ of a hyperbola such that its foci will be located at z_{OP} and z_{F_2}, subject to the condition that the asymptotic slope of the hyperbola will be $m_A = 3°$. After reflection from this hyperbola, the ray considered in Step 1 will pass through the focal point z_{F_2} of the telescope. Compute the point of intersection (x_{3MIN}, z_{3MIN}) of the ray with this hyperbola. This point

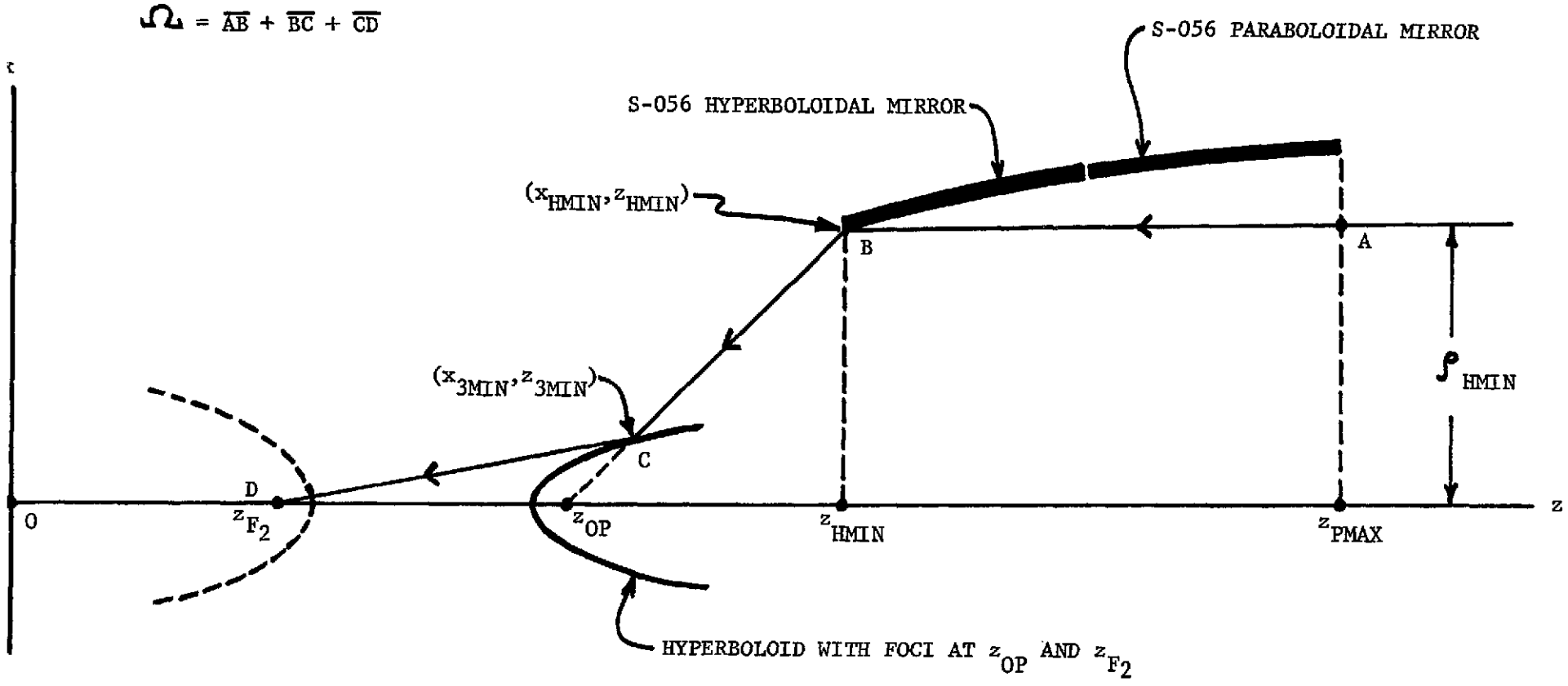

Figure 3. Determination of the reference optical path length Ω for elimination of spherical aberration.

is the initial point on the aspheric third mirror.

(3) Since the ray considered above is successfully imaged at z_{F_2} by the H-A channel, its optical path length can be taken as the reference optical path length for all other rays traversing the H-A channel. If this optical path length is denoted by Ω, then

$$\Omega = \overline{AB} + \overline{BC} + \overline{CD}$$

where

$$\overline{AB} = z_{PMAX} - z_{HMIN}$$

$$\overline{BC} = \left[(x_{HMIN} - x_{3MIN})^2 + (z_{HMIN} - z_{3MIN})^2 \right]^{1/2}$$

$$\overline{CD} = \left[x_{3MIN}^2 + (z_{3MIN} - z_{F_2})^2 \right]^{1/2}.$$

The numerical value of Ω is found to be

$$\Omega = 79.8236419647 \text{ inches.} \qquad (4)$$

(4) Using the value of Ω in Eq. (4), it is now necessary to impose the condition that all other incoming rays parallel to the optical axis traverse the same optical path length in the H-A channel. Suppose, as shown in Fig. 4, that an arbitrary ray strikes the S-056 hyperboloidal mirror at (x_H, z_H). After reflection from the hyperboloidal mirror, it strikes the aspheric third mirror at point P_3 - - the coordinates (x_3, z_3) of which are to be determined by equalization of optical path lengths -- and is then reflected through the focal point z_{F_2}. Two conditions can be im-

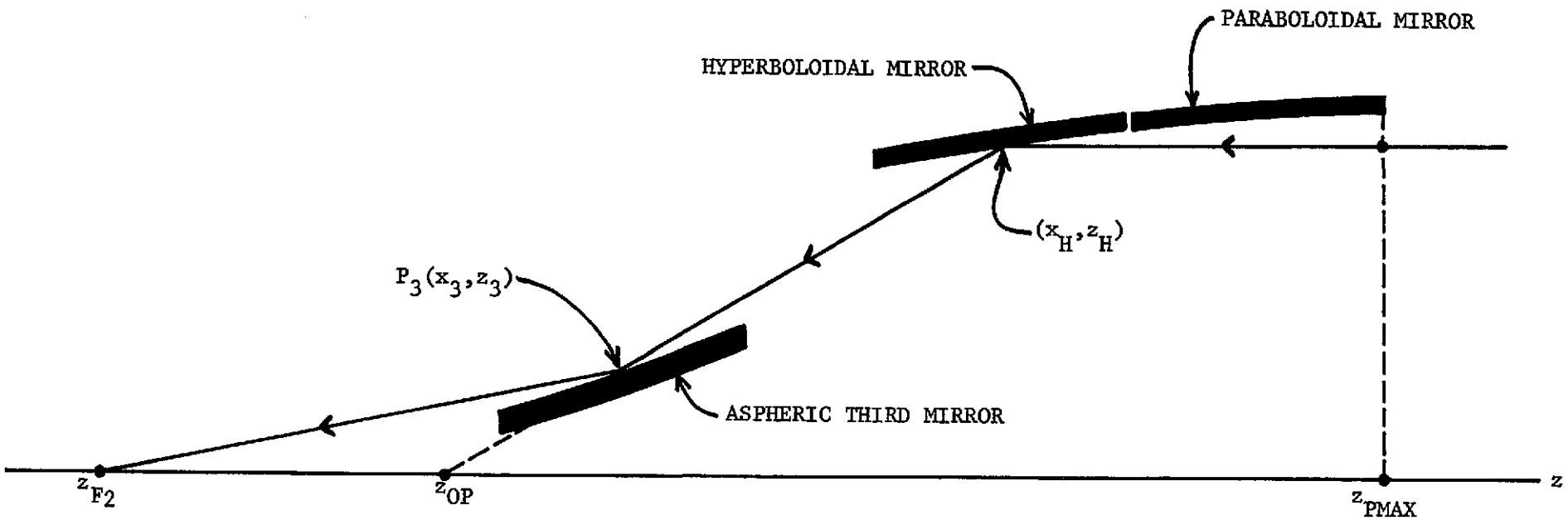

Figure 4. Generation of points (x_3,z_3) on the aspheric third mirror by equalization of optical path lengths.

posed on point P_3. First, it must lie on the ray reflected from the hyperboloidal mirror at (x_H, z_H). Second, the total optical path length for the ray, from the point at which it enters the telescope at $z = z_{PMAX}$ until it reaches the focal point z_{F_2}, must be equal to the reference optical path length Ω in Eq. (4). Mathematical implementation of these two conditions yields two equations which determine x_3 and z_3. Carrying out this procedure for incoming rays at various distances from the optical axis out to ρ_{HMAX} gives a set of discrete points which lie on the surface of the aspheric third mirror. This set of points must be fitted with a continuous curve before the system can be ray traced.

Mathematical implementation of Step 4 proceeds as follows. Inspection of Fig. 4 shows that the equation of the ray leaving (x_H, z_H) is

$$x = \frac{x_H}{z_H - z_{OP}} (z - z_{OP}) , \tag{5}$$

where z_{OP} can be calculated by the ray trace methods in Appendix A of Ref. 1. For brevity, let

$$\sigma = \frac{x_H}{z_H - z_{OP}} .$$

Then Eq. (5) becomes

$$x = \sigma (z - z_{OP}) .$$

Since the point (x_3, z_3) on the aspheric mirror must lie on this ray, it is then necessary that

$$x_3 = \sigma (z_3 - z_{OP}) . \tag{6}$$

The second condition on (x_3, z_3) is that the optical path length for the ray must equal the value for Ω given in Eq. (4). From Fig. 4 it is evident that the optical path length, measured from the plane $z = z_{PMAX}$, is

$$O.P.L. = z_{PMAX} - z_H + \left[(x_H - x_3)^2 + (z_H - z_3)^2 \right]^{1/2} + \left[x_3^2 + (z_3 - z_{F_2})^2 \right]^{1/2} .$$

Setting the OPL equal to Ω then gives

$$\Omega = z_{PMAX} - z_H + \left[(x_H - x_3)^2 + (z_H - z_3)^2 \right]^{1/2} + \left[x_3^2 + (z_3 - z_{F_2})^2 \right]^{1/2} . \tag{7}$$

Eqs. (6) and (7) constitute two simultaneous equations in the two unknowns x_3 and z_3. Substitution of Eq. (6) into Eq. (7) produces a quadratic

equation in z_3:

$$A_3 z_3^2 + B_3 z_3 + C_3 = 0, \tag{8}$$

with

$$A_3 = 4\left(\eta^2 - \tau^2\right)$$

$$B_3 = -4\left(\mu^2 \tau + 2\eta^2 z_H\right)$$

$$C_3 = 4\eta^2 z_H^2 - \mu^4 ,$$

where

$$\eta^2 = \lambda^2 (\sigma^2 + 1)$$

$$\tau = z_{F_2} - \sigma \chi_H - z_H$$

$$\lambda = \Omega - z_{PMAX} + z_H$$

$$\mu^2 = \lambda^2 + \chi_H^2 + z_H^2 - z_{F_2}^2 + 2\sigma \chi_H z_{OP} .$$

The physically relevant solution of Eq. (8) is

$$z_3 = \frac{-B_3 - \left(B_3^2 - 4A_3 C_3\right)^{1/2}}{2A_3} . \tag{9}$$

Once z_3 has been computed from Eq. (9), x_3 can be obtained from Eq. (6).

In order to obtain a set of numerical values for points (x_3,z_3) on the aspheric third mirror, 101 rays equally spaced from $\int_{HMIN}$ to $\int_{HMAX}$ were traced through the H-A channel, and 101 corresponding sets of coordinates (x_3,z_3) were obtained as outlined above. The coordinates of the initial point are $x_3(0) = 0.9275547837$, $z_3(0) = 107.6315216613$ (all values are in inches), while the coordinates of the final point are $x_3(100) = 1.3148183528$, $z_3(100) = 113.6988785788$. The average radius of the mirror is 1.12 inches, and the mirror is 6.07 inches long.

Ray Trace Analysis

In the usual aspheric ray trace procedure[4], the aspheric optical surface to be ray traced is approximated by a sphere centered on the optical axis, plus a power series in the radial variable. In the present case, however, no sphere centered anywhere on the optical axis would represent a reasonable approximation to the shape of the aspheric third mirror. A fresh mathematical approach is therefore required.

The aspheric third mirror is slightly concave, as the drawing in Fig. 5 suggests. In order to approximate the aspheric mirror shape, a parabola of the form

$$x - x_0 = C\,(z - z_0)^2 \tag{10}$$

was used, where C is a constant and (x_0, z_0) are the coordinates of the vertex of the parabola. The constants C, x_0, and z_0 were adjusted (more or less by trial and error) until the parabola and the aspheric were less than 100 waves apart in the z-direction for any $x_3(0) \leq x \leq x_3(100)$. The resulting values were

$$x_0 = -3.780719371 \text{ inches}$$

$$z_0 = -42.81997126 \text{ inches}$$

$$C = 1.040012943 \times 10^{-4} \text{ inches}^{-1}.$$

Using this parabola as a geometrical approximation to the aspheric, a power series fit of the form

$$z_{\text{ASPHERIC}} = z_{\text{PARABOLA}} + \sum_{n=1}^{5} c_n x^n \tag{11}$$

was made to the 101 discrete points $x_3(i)$, $z_3(i)$ $\left[i = 0,1,2,\ldots,100\right]$

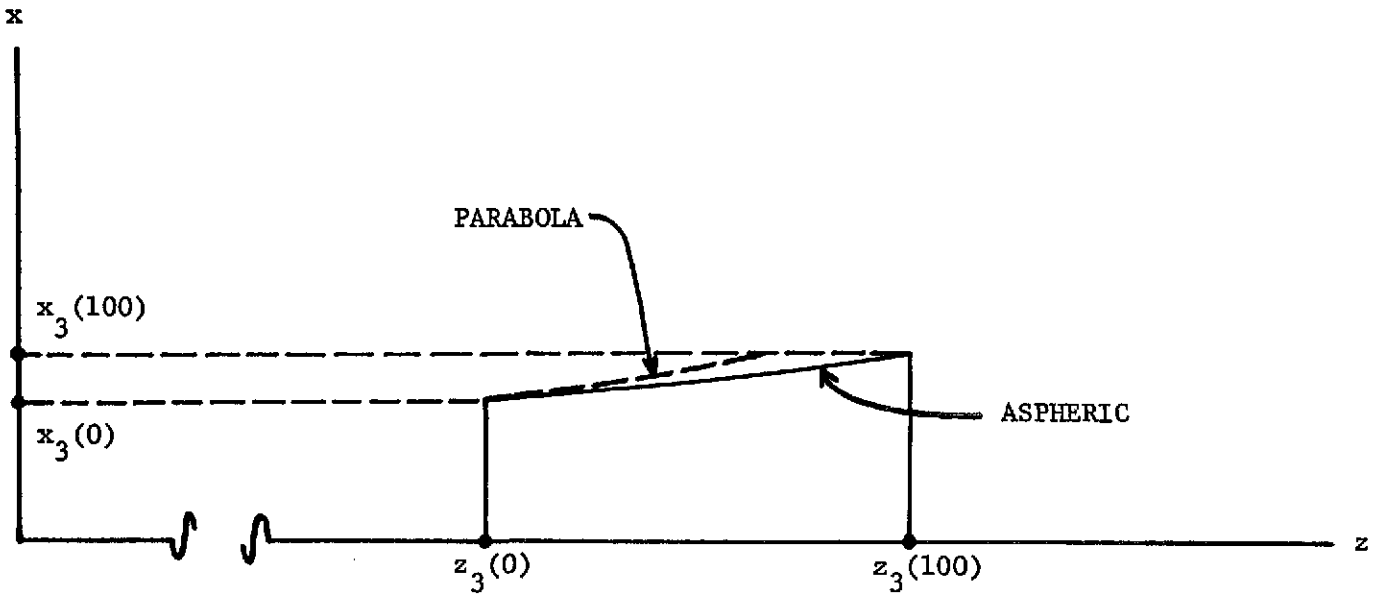

Figure 5. Approximation of the aspheric third mirror by a parabola.

on the aspheric generated earlier. In Eq. (11),

$$X = x_3 - x_3(0)$$

and, from Eq. (10),

$$z_{PARABOLA} = z_0 + \left(\frac{x_3 - x_0}{C} \right)^{1/2} .$$

The constants C_n in Eq. (11) were evaluated by the method of least squares[5]. The resulting values are:

$$C_1 = 2.045750497 \times 10^{-2}$$

$$C_2 = -0.1255184228$$

$$C_3 = 0.2736987956$$

$$C_4 = -0.1445566312$$

$$C_5 = 4.846699896 \times 10^{-2}.$$

When these constants are used, Eq. (11) fits the aspheric mirror surface to an accuracy better than 1/100 wavelength at λ = 5500 Å.

Using Eq. (11) as the mathematical representation of the aspheric third mirror, Feder's ray trace procedure[4] can be carried out in standard fashion, with modifications where necessary because of the specialized form of Eq. (11).

The aspheric mirror has also been ray traced using a spline function representation[6]. In this case, a cone of revolution about the optical axis, passing through the endpoints $(x_3(0), z_3(0))$ and $(x_3(100), z_3(100))$ of the

mirror, can be used as a geometrical approximation to the aspheric. In general, the spline function representation appears to give more accurate results than the power series representation.

Imaging Characteristics

The H-A channel of the TMXRT has been ray traced using both Feder's method (i.e., the power series representation) and the spline function representation, with excellent agreement between the two. Since the original aspheric third mirror was designed to eliminate spherical aberration, the spot size in the focal plane for an on-axis point source at infinity should be zero (ignoring diffraction). In practice, a geometrical ray trace will produce a very small, but finite, spot size for this case. There are two reasons for this. First, the mathematical representation of the aspheric mirror surface -- whether it be a power series or a spline function -- will not coincide exactly at every point with the actual mirror surface itself. Second, even if the mathematical representation used for the aspheric mirror were perfect, the digital computer running the ray trace program can only work with a limited number of significant digits, and is thus subject to some roundoff error. In order to minimize the second factor, all ray trace programs for the TMXRT have been run in the automatic double precision mode on the XDS-Sigma 5 computer. It has been found that the spline function representation gives a smaller on-axis spot size than the power series representation (by about two orders of magnitude), and it therefore appears that the spline function representation is the more accurate of the two. For off-axis images, both representations give identical results.

Table III gives the rms diameter of the spot formed in the focal plane by the H-A channel as a function of off-axis angle for a point source at

infinity. Also listed in Table III is the approximate spot diameter expressed in minutes of arc for each off-axis angle. These values are only approximate, because the effective focal length of the H-A channel varies with off-axis angle (the H-A channel is badly afflicted with coma). The effective focal length varies from approximately 161 inches for rays which strike the hyperboloidal mirror at a radius of f_{HMIN} to approximately 141 inches for rays which strike the hyperboloidal mirror at a radius of f_{HMAX}. The data in column three of Table III were computed using a constant average effective focal length of 150 inches for the H-A channel. Inspection of Table III shows that the H-A channel is indeed free from spherical aberration (the on-axis spot size is for practical purposes, zero), but that coma causes the spot size to increase rapidly with off-axis angle.

It might be supposed that curvature of field, as well as coma, plays a significant role in determining the off-axis spot size. In order to study the effects of field curvature in the H-A channel, a computer program was written to calculate the rms spot diameter in various planes near the focal plane for any given off-axis angle. Use of the data from this program allowed the plane of best focus to be approximately determined as a function of off-axis angle. The results are summarized in Table IV. It would appear from the data in Table IV that the H-A channel suffers from a very large curvature of field. At an off-axis angle of 6 arc-minutes, for example, the plane of best focus is 0.65 inch in front of the focal plane (notice that the surface of best focus for the H-A channel bends <u>toward</u> the paraboloid-hyperboloid mirror assembly, as it also does for the P-H channel). This behavior may be contrasted with that for the P-H channel,

Table III. Spot diameter as a function of off-axis angle for the H-A channel, with the aspheric third mirror designed to eliminate spherical aberration.

OFF-AXIS ANGLE (arc-minutes)	RMS SPOT DIAMETER (millimeters)	RMS SPOT DIAMETER (arc-minutes)
0.0	1.78×10^{-6}	1.60×10^{-6}
2.0	1.64	1.48
4.0	3.30	2.98
6.0	4.96	4.48

Table IV. Plane of best focus as a function of off-axis angle for the H-A channel of the TMXRT, with the aspheric third mirror designed to eliminate spherical aberration.

OFF-AXIS ANGLE (arc-minutes)	Z-COORDINATE OF PLANE OF BEST FOCUS (INCHES) *
0.0	75.00
0.5	75.00
1.0	75.00
1.5	75.05
2.0	75.10
2.5	75.10
3.0	75.15
3.5	75.25
4.0	75.30
4.5	75.35
5.0	75.45
5.5	75.60
6.0	75.65

*Results expressed to the nearest 5/100 inch.

in which the plane of best focus at 6 arc-minutes is only about 0.007 inch in front of the focal plane[7]. The strong field curvature suggested by the data in Table IV is highly misleading, however, because the spot size for a given off-axis angle in the H-A channel varies quite slowly as a function of z. For example, at an off-axis angle of 6 arc-minutes, the rms spot diameter in the focal plane (z = 75.00 inches) is 4.96 mm, while in the plane of best focus (z = 75.65 inches) the rms spot diameter is 4.85 mm. Moving from the focal plane to the plane of best focus at 6 arc-minutes therefore results in a decrease of only 0.11 mm in the spot diameter (a 2% net decrease). Therefore it is clear that the rapid increase in spot size with off-axis angle in the H-A channel is due almost entirely to coma, and that field curvature plays a negligible role.

Unfortunately, the image of an off-axis point source at infinity formed in the focal plane by the H-A channel is not a solid spot; the spot has a hole in the middle. Fig. 6 shows a tracing of the spot diagram in the focal plane for an off-axis angle of 2 arc-minutes, for example. The hole in the middle of the spot is caused by coma, not by curvature of field. A spot diagram in the plane of best focus at 2 arc-minutes looks exactly like that in Fig. 6.

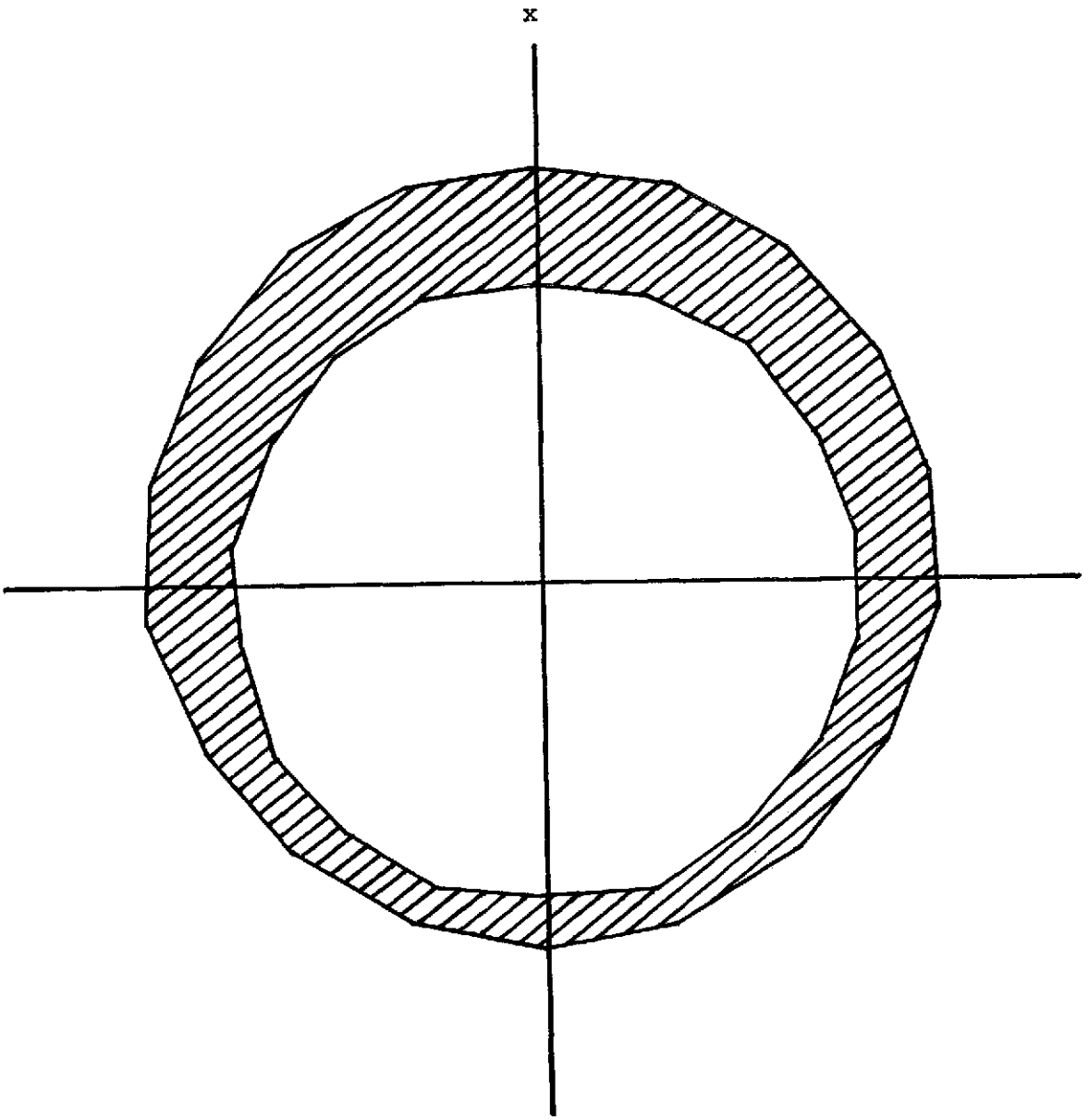

Figure 6. Tracing of the spot diagram in the focal plane for an off-axis angle of 2 arc-minutes.

Tilt and Decentration Sensitivity

The behavior of the H-A channel of the TMXRT under decentration and angular tilt of the aspheric third mirror has been investigated to assure that the system is not impractically sensitive to mechanical assembly errors. The general approach used to ray trace the system when decentration or tilt is present has already been documented[8].

Qualitatively, both decentration and tilt of the aspheric mirror produce a spot with a hole in the center, very much like the off-axis spots produced by the perfectly aligned system. Fig. 7 shows, for example, the spot which results from a decentration of 0.001 inch.

Quantitative information on spot size as a function of decentration or tilt is summarized in Tables V and VI. The spot diameters expressed as arc-seconds in these two tables were obtained using an average effective focal length of 150 inches. It will be observed from the data in Tables V and VI that the spot diameter is a linear function of decentration or angular tilt.

The numbers in parentheses in column three of Tables V and VI give the spot diameter in arc-seconds for an equivalent decentration or tilt of the hyperboloidal mirror in the S-056 telescope. Comparison of these numbers with the corresponding results for the H-A channel shows that the aspheric third mirror is roughly twice as sensitive to decentration as the hyperboloidal mirror in S-056, but only about one-third as sensitive to angular tilt.

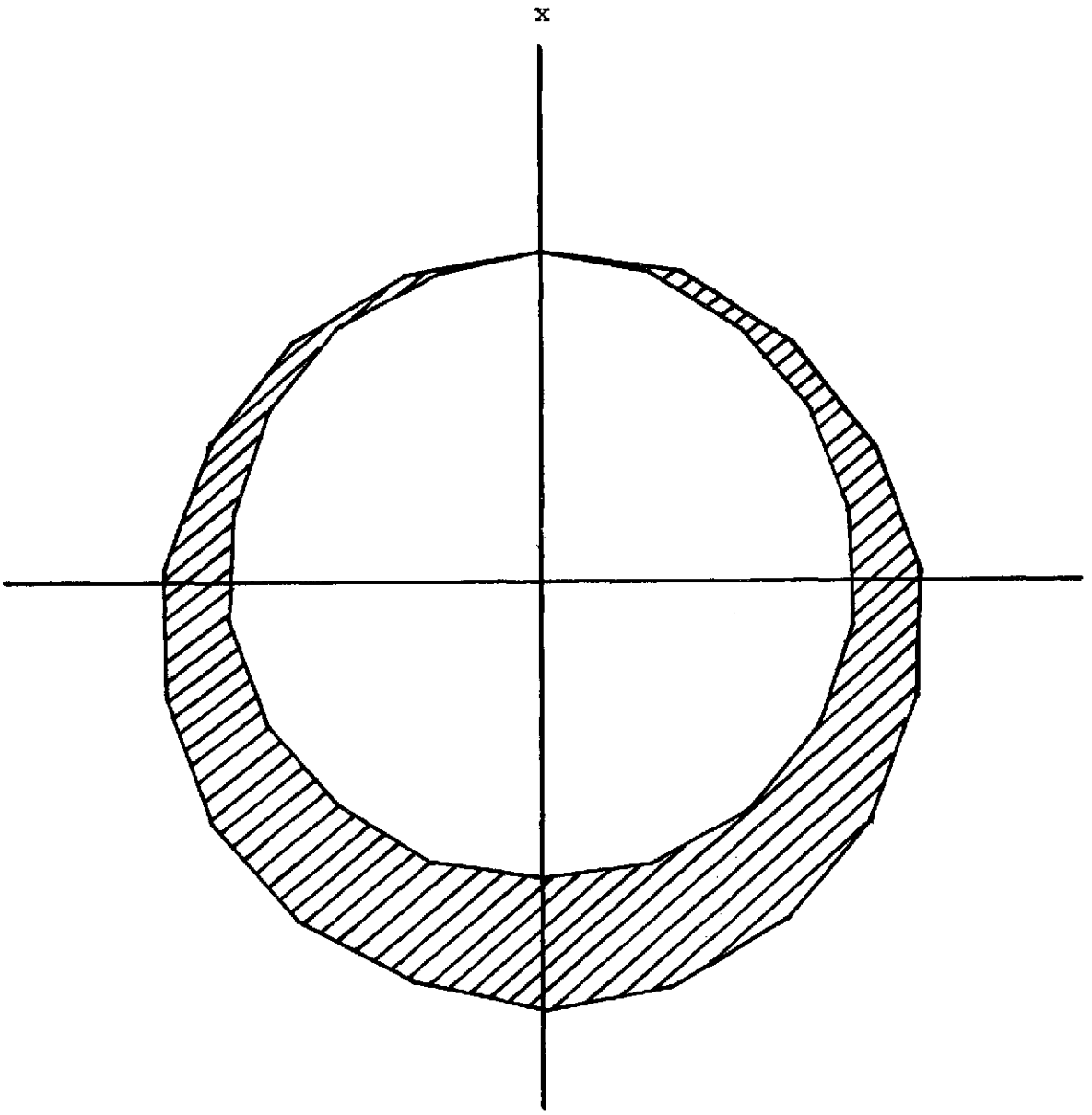

Figure 7. Tracing of the spot diagram showing the image in the focal plane of an on-axis point source at infinity when the aspheric third mirror is decentered by 0.001 inch.

Table V. Spot diameter in the focal plane as a function of decentration of the aspheric third mirror.

DECENTRATION (inches)	SPOT DIAMETER (inches)	SPOT DIAMETER (arc-seconds)
0.0001	3.93×10^{-4}	0.54
0.0005	1.97×10^{-3}	2.71
0.0010	3.94×10^{-3}	5.42 (2.75)*
0.0050	1.96×10^{-2}	27.0 (13.8)
0.0100	3.91×10^{-2}	53.8 (27.5)

*Results in parentheses refer to decentration of the hyperboloidal mirror in S-056.

Table VI. Spot diameter in the focal plane as a function of angular tilt of the aspheric third mirror.

ANGULAR TILT (arc-seconds)	SPOT DIAMETER (inches)	SPOT DIAMETER (arc-seconds)
1.0	4.87×10^{-4}	0.67
2.0	9.75×10^{-4}	1.34 (4.68)*
4.0	1.95×10^{-3}	2.68
6.0	2.92×10^{-3}	4.02 (12.4)
8.0	3.90×10^{-3}	5.36
10.0	4.87×10^{-3}	6.70 (20.1)

*Results in parentheses refer to angular tilt of the hyperboloidal mirror in S-056.

Optimum Aspheric Mirror Location

The location for the aspheric third mirror was chosen on the basis of producing a mirror of reasonable size, not on the basis of producing the best possible imaging characteristics. However, it is certainly desirable to know where the aspheric mirror should be located along the optical axis in order to optimize the image produced in the focal plane by the H-A channel.

In order to determine the effect, if any, of relocating the aspheric third mirror, six new locations were selected, two between the original mirror location and the hyperboloid pseudo-focus (HPF), and four between the original mirror location and the S-056 mirror assembly. As soon as z_{3MIN} had been selected for each location, the corresponding value of x_{3MIN} was automatically determined by the requirement that the point (x_{3MIN}, z_{3MIN}) lie on the ray reflected from the S-056 hyperboloidal mirror at (x_{HMIN}, z_{HMIN}). At each mirror location, a complete aspheric mirror designed to eliminate spherical aberration was generated by the method described earlier. Table VII summarizes the basic parameters for the various mirrors (mirror #3 is the original mirror, included for handy reference).

It will be observed from Table VII that the aspheric mirror becomes larger in diameter and longer as it is moved from the HPF toward the S-056 mirror assembly. The average glancing angle of incidence decreases as the aspheric mirror is moved toward the S-056 mirror assembly.

Each mirror listed in Table VII was ray traced using the spline function technique, and the rms spot diameter in the focal plane was calculated as a function of off-axis angle. Fig. 8 summarizes these ray trace results graphically. Inspection of Fig. 8 shows that the spot diameter is a linear

Table VII. Basic parameters for relocated aspheric third mirrors.

	x_{3MIN} (inches)	z_{3MIN} (inches)	x_{3MAX} (inches)	z_{3MAX} (inches)	Mirror Length (inches)	Nominal Mirror Diameter (inches)	Average Glancing Angle of Incidence (degrees)	Average Focal Length (inches)
#1	0.309	101.239	0.576	106.020	4.781	0.880	2.30	323.2
#2	0.618	104.435	0.945	109.853	5.418	1.557	2.05	197.3
#3	0.928	107.632	1.315	113.699	6.067	1.118	1.85	151.0
#4	1.536	113.919	2.046	121.299	7.380	3.574	1.55	112.2
#5	2.144	120.206	2.782	128.947	8.741	4.916	1.33	94.7
#6	2.752	126.493	3.522	136.642	10.149	6.262	1.16	84.8
#7	3.360	132.780	4.268	144.386	11.606	7.613	1.04	78.3

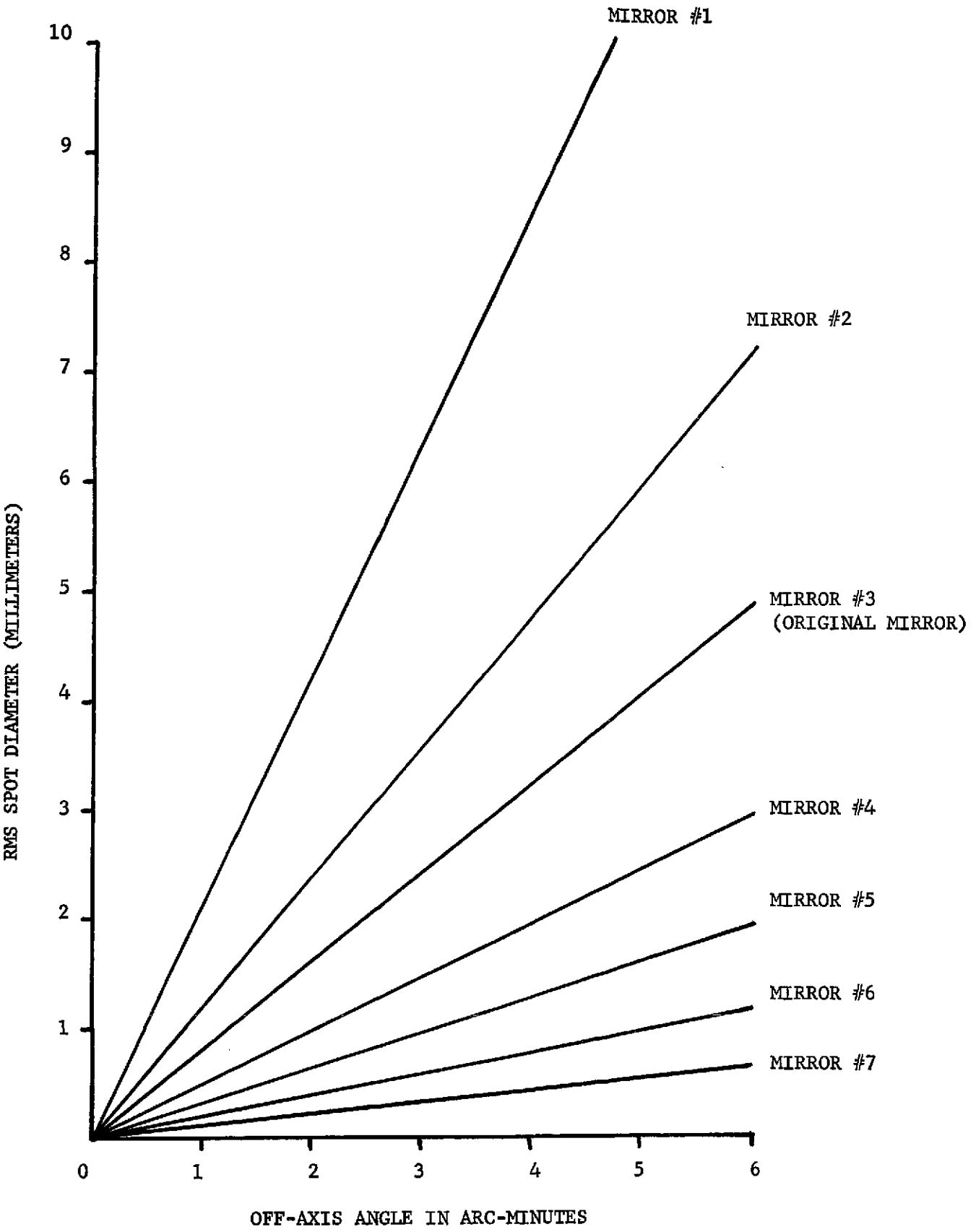

Figure 8. Spot size as a function of off-axis angle for various aspheric third mirror locations.

function of off-axis angle over a ± 6 arc-minute field of view, and that the spot diameter at a given off-axis angle decreases dramatically as the aspheric mirror is moved toward the S-056 mirror assembly (i.e., as the assigned mirror number increases). The optimum location for the aspheric third mirror from the viewpoint of image quality is therefore as close to the S-056 mirror assembly as possible. Mirror #7, having z_{3MAX} = 144.386 inches, is almost as far forward as possible without projecting beyond the rear of the S-056 hyperboloidal mirror (the rear of the S-056 hyperboloidal mirror is at z_{HMIN} = 145.354 inches). There would be a 0.968 inch clearance between the front of mirror #7 and the rear of the S-056 hyperboloidal mirror.

Since the spot size for mirror #7 at any given off-axis angle is much smaller than that for the original mirror (by roughly a factor of 8), signifying that mirror #7 is much less afflicted with coma, it might be expected that the hole in the center of a typical spot would be less pronounced for mirror #7 than for the original mirror. This conjecture was checked out by plotting some off-axis spot diagrams for mirror #7. Fig. 9 shows the spot diagram in the focal plane for an off-axis angle of 2 arc-minutes. Comparison of this spot with the corresponding spot produced by the original mirror, shown in Fig. 6, shows that the spot produced by mirror #7 is indeed much more filled out than that produced by the original mirror.

It should be pointed out that the effective focal length of the H-A channel will depend on the placement of the aspheric third mirror. As the aspheric mirror moves closer to the S-056 mirror assembly, the average effective focal length of the H-A channel decreases, as shown in the final column of Table VII. Thus, the dramatic decrease in spot size from mirror #1 to mirror #7 will not be accompanied by such an equally dramatic increase in angular

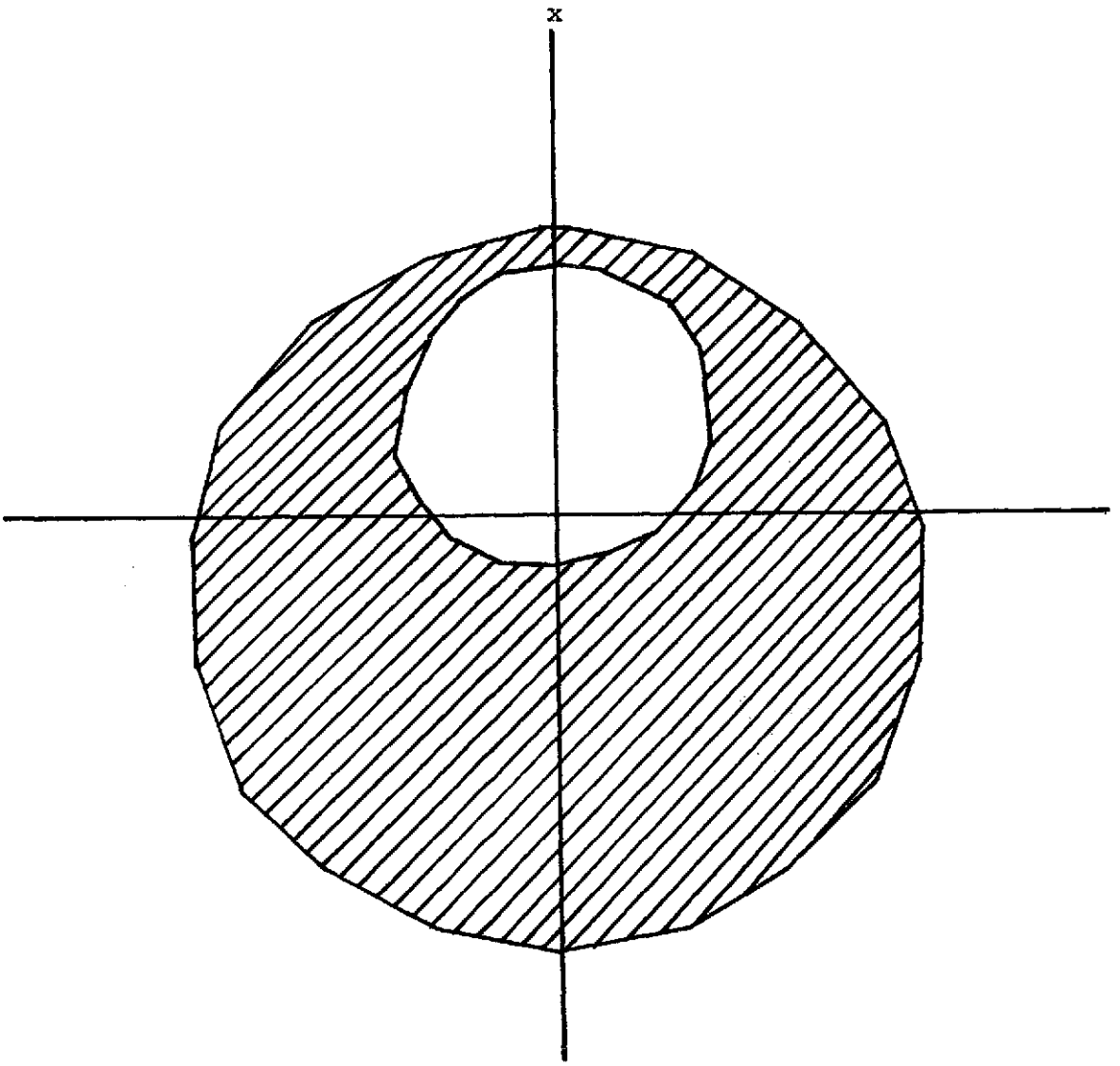

Figure 9. Tracing of the spot diagram in the focal plane for mirror #7 for an off-axis angle of 2 arc-minutes.

resolution, because the effective focal length of mirror #7 will be smaller than that of mirror #1. While this point should be recognized, it is not of primary importance, since the finite size of the position-sensitive proportional counter cells (1 x 4 millimeters) ultimately sets the limit on the angular resolution of the TMXRT. It is only necessary for the H-A channel to form a spot whose diameter is less than 1 mm over the entire field of view in order to be "matched" to the detector array. Mirror #6 achieves this goal over a $\pm$ 5 arc-minute field of view, while mirror #7 would achieve the same result over a field of view of approximately $\pm$ 10 arc-minutes.

While mirrors #1 through #7 do not suffer any vignetting for an on-axis point source at infinity, there will be some vignetting for off-axis point sources. A rough idea of the amount of vignetting at a given off-axis angle can be obtained by calculating the percentage of rays entering the aperture of the H-A channel (i.e., from $\int_{HMIN}$ to $\int_{HMAX}$) which fail to strike either the hyperboloidal mirror or the aspheric third mirror. Table VIII summarizes vignetting data obtained by this oversimplified method for the various mirrors. Inspection of the data in Table VIII reveals that vignetting at small off-axis angles is slightly smaller for mirror #7 than for mirror #1, but that at larger off-axis angles the vignetting is greatly reduced in going from mirror #1 to mirror #7. Thus, moving the aspheric third mirror as close as possible to the S-056 mirror assembly simultaneously produces minimum vignetting and maximum image quality. With these facts in mind, it may be that the extra cost of fabricating a large aspheric third mirror which mounts directly behind the S-056 mirrors can be justified in order to obtain the best possible performance from the H-A channel of the TMXRT.

Table VIII. Roughly estimated percentage vignetting for the relocated aspheric third mirrors as a function of off-axis angle.

Off-Axis Angle (arc-minutes)	Amount of Vignetting (%)						
	Mirror #1	Mirror #2	Mirror #3	Mirror #4	Mirror #5	Mirror #6	Mirror #7
0	0	0	0	0	0	0	0
1	9.5	9.5	9.5	9.5	9.5	9.5	8.9
2	14.7	14.2	12.6	10.5	9.5	9.5	9.5
3	18.4	17.4	15.8	14.7	12.1	10.5	9.5
4	22.6	22.1	20.5	17.9	14.7	12.1	11.1
5	27.9	25.3	24.7	21.1	17.9	14.2	12.1
6	32.6	30.5	27.9	24.2	18.9	16.3	12.6

IV. OTHER MIRROR DESIGNS

The aspheric third mirror discussed above was designed to eliminate spherical aberration in the H-A channel, with no attempt to control coma. Since the "primary" mirror of the H-A channel is constrained to be hyperboloidal, only one mirror surface -- that of the aspheric third mirror -- can be manipulated for optical design purposes. With only one free surface available, spherical aberration and coma can not be eliminated simultaneously to make the H-A channel truly aplanatic, although each aberration can be eliminated separately with no control over the other (except such control as can be obtained by repositioning the aspheric mirror, or by use of intentional vignetting). In order to explore the full range of possibilities for the H-A channel, an aspheric third mirror has been designed which is free from coma. The properties of this mirror will now be discussed.

If coma is to be eliminated, the H-A channel must be constrained to obey the Abbe sine condition. In the case of a telescopic system, the sine condition requires that the quantity $h/\sin\theta$ be constant for all rays traversing the system, where h is the distance from the path of the incoming ray to the optical axis (all incoming rays are to be parallel to the optical axis), and θ is the angle the ray makes with the optical axis on its way to the focal point of the telescope. A coma-free aspheric mirror for the H-A channel of the TMXRT was designed as follows.

(1) The point (x_{3MIN}, z_{3MIN}) was chosen to be the same as for the original mirror designed to eliminate spherical aberration, so that the coma-free mirror would be of comparable size to the original mirror. Starting with a ray reflected from the hyperboloidal

mirror at ρ_{HMIN} and assuming this ray passes through the focal point z_{F_2} after reflection from the aspheric mirror at (x_{3MIN}, z_{3MIN}), the focal length $f_1 = h_1/\sin\theta_1$ for this ray was calculated (see Fig. 10). The distance $h_1 = \rho_{HMIN}$ is known, and θ_1 can be found by use of some elementary trigonometry:

$$\theta_1 = \tan^{-1}\left(\frac{x_{3MIN}}{z_{3MIN} - z_{F_2}}\right).$$

(2) For an adjacent ray entering the TMXRT at a distance h_2 from the optical axis, the sine condition requires that the focal length $f_2 = h_2/\sin\theta_2$ be identical to that for the first ray:

$$\frac{h_2}{\sin\theta_2} = \frac{h_1}{\sin\theta_1}.$$

The angle θ_2 is thus required to have the value

$$\theta_2 = \sin^{-1}\left(\frac{h_2}{h_1}\sin\theta_1\right).$$

However, the point of intersection z_2 of this ray with the optical axis is unknown. (If spherical aberration and coma could be eliminated simultaneously, then all rays would be required to pass through the same point z_{F_2}, and the focal length for all rays would be constant and equal to f_1. In that case, the principal

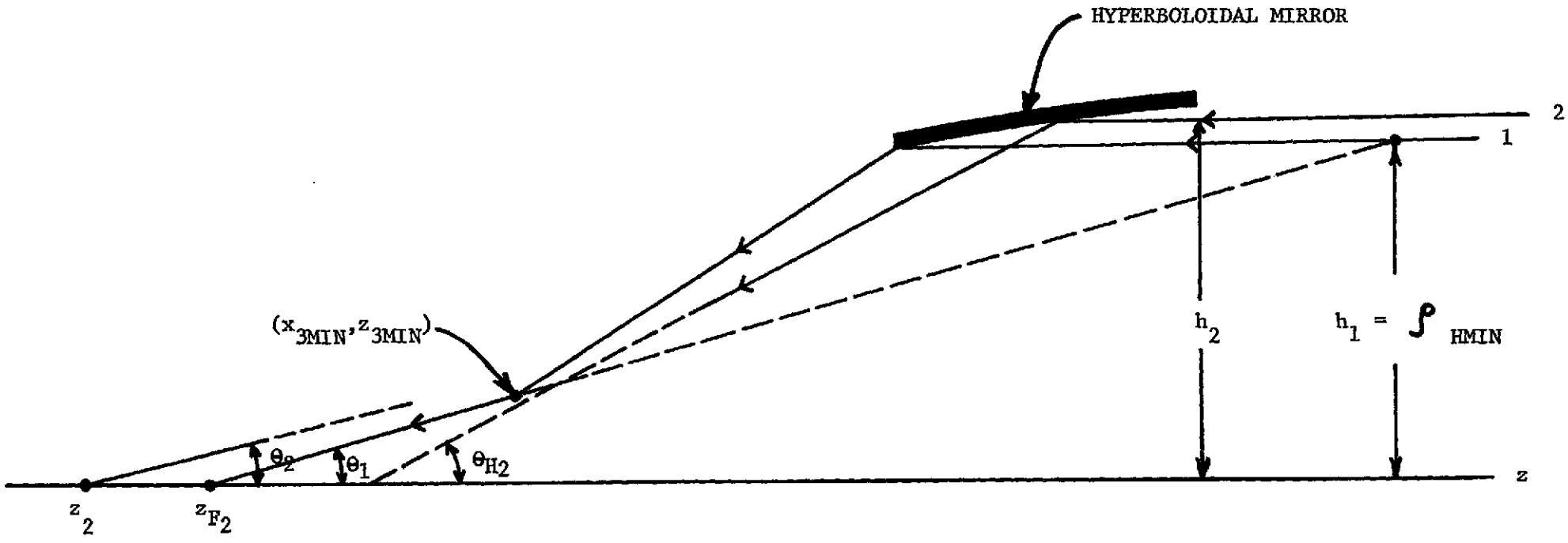

Figure 10. Generation of the coma-free aspheric third mirror.

surface would be a sphere of radius f_1 centered at z_{F_2}. In the present case, however, we do not have the freedom to impose both conditions simultaneously. If the second ray is required to have the same focal length as the first, it therefore can not be required to come to focus at the same point on the optical axis as the first ray.)

(3) The coordinates $\left[x_{3M}(2),\ z_{3M}(2)\right]$ of the point at which the second ray is reflected from the aspheric mirror are unknown. However, the slope which the aspheric mirror must have at this point can be determined. If the second ray makes an angle Θ_{H_2} with the optical axis on its way to the aspheric mirror, and makes an angle Θ_2 with the optical axis after reflection from the aspheric mirror, then the law of reflection requires that the aspheric mirror surface itself at the point of reflection must make an angle $\Theta_{3M}(2) = \frac{1}{2}(\Theta_{H_2} + \Theta_2)$ with the optical axis. The slope of the aspheric mirror surface at $\left[x_{3M}(2),\ z_{3M}(2)\right]$ must therefore be tan $\Theta_{3M}(2)$.

(4) In order to generate the coordinates $\left[x_{3M}(2),\ z_{3M}(2)\right]$, a line starting at $(x_{3MIN},\ z_{3MIN})$ with slope equal to tan $\Theta_{3M}(2)$ was constructed, and its intersection with the second ray after reflection from the hyperboloidal mirror was found. The coordinates of this intersection are an approximation to the required coordinates $\left[x_{3M}(2),\ z_{3M}(2)\right]$. In effect, a mirror is generated in this way whose average slope between $(x_{3MIN},\ z_{3MIN})$ and $\left[x_{3M}(2),\ z_{3M}(2)\right]$

is equal to the exact slope required at $\left[x_{3M}(2),\ z_{3M}(2)\right]$. If the first and second rays are taken sufficiently close together, the approximation should be satisfactory.

(5) The remaining points on the coma-free aspheric third mirror were determined by successive repetitions of the procedure described in Step 4, starting with the second point in order to generate the third, the third in order to generate the fourth, etc. One hundred and one discrete points were generated. The initial point, as mentioned above, was the same as the initial point on the original mirror, with coordinates $x_3(0) = 0.9275547837$ and $z_3(0) = 107.6315216613$ (all values in inches). The final point has coordinates $x_3(100) = 1.2954762562$ and $z_3(100) = 113.4978566730$. The mirror is 5.87 inches long and has a nominal diameter of 2.22 inches. The coma-free mirror is slightly shorter than the original mirror.

The coma-free mirror was ray traced using the spline function technique. Table IX summarizes the results obtained for the rms spot diameter in the focal plane as a function of off-axis angle. The effective focal length of the H-A channel utilizing the coma-free mirror is constant for all rays and equal to 161.0 inches. The large on-axis spot size shows that severe spherical aberration is present. However, the slow rate of increase of spot size with off-axis angle indicates that coma has been significantly reduced.

Owing to the large amount of spherical aberration which it exhibits, the coma-free mirror would not produce on-axis images with acceptable resolution. However, the focal plane of the telescope (located at $z_{F_2} = 75.0$ inches) is not the plane of best on-axis focus for the coma-free mirror.

Table IX. Spot diameter in the focal plane as a function of off-axis angle for the H-A channel incorporating the coma-free aspheric third mirror.

OFF-AXIS ANGLE (arc-minutes)	RMS SPOT DIAMETER (millimeters)	RMS SPOT DIAMETER (arc-minutes)
0.0	4.09	3.44
2.0	4.61	3.88
4.0	5.06	4.25
6.0	5.75	4.83

The on-axis resolution could be improved somewhat by moving to the plane in which the circle of least confusion is located (z = 72.40 inches, approximately). The on-axis spot diameter in this plane is 2.35 millimeters (1.98 arc-minutes), which is 43% smaller than the on-axis spot diameter in the focal plane of the telescope, but still unacceptably large.

It would be natural to expect the coma-free mirror to produce spots which are solid. In order to check this conclusion, spot diagrams were plotted for the coma-free mirror system in the plane of best on-axis focus. Fig. 11 shows spot diagrams in this plane for the on-axis case, and also for an off-axis angle of 2.0 arc-minutes. As expected, the spots are solid.

A number of compromise mirrors, intermediate between the original mirror and the coma-free mirror, were generated and ray traced to see if a reasonable balance could be obtained between spherical aberration and coma. The 101 points on each compromise mirror surface were generated by a fixed linear interpolation between corresponding points on the original mirror and the coma-free mirror. It was found that even a small departure from the original mirror gives rise to unacceptably large spherical aberration, so the use of compromise mirrors was not pursued further. Chronologically, the compromise mirrors were generated before the effects of repositioning the original mirror had been determined. Actually, the performance of the original mirror when located directly behind the S-056 hyperboloidal mirror is so good that, had this been known earlier, generation of compromise mirrors would probably never have been undertaken.

The outermost rings of spots in Fig. 11A are produced by rays that strike the hyperboloidal mirror near its maximum radius ρ_{HMAX}. After reflection from the hyperboloidal mirror, these rays strike that segment of

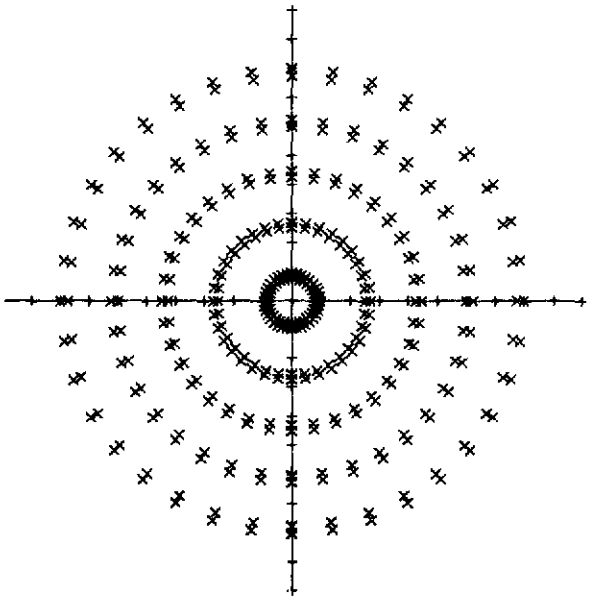

A. Off-axis angle = 0

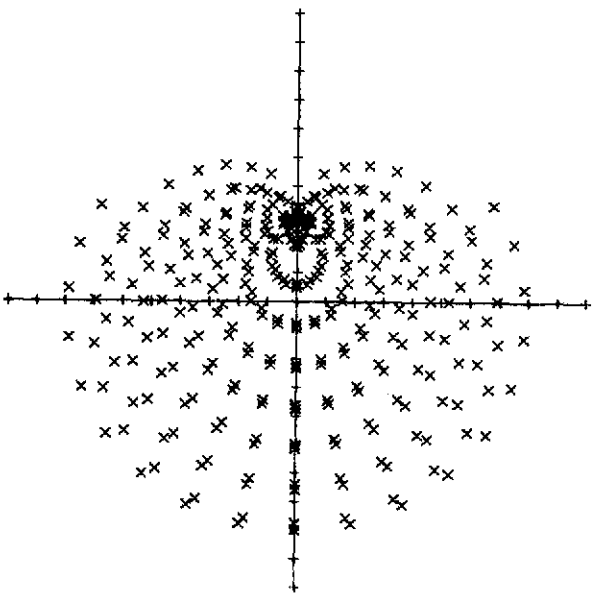

B. Off-axis angle = 2.0 arc-minutes

Figure 11. Spot diagrams in the plane of best on-axis focus (z = 72.40 in.) for the coma-free mirror.

the aspheric mirror near z_{3MAX}. If these rays were intentionally vignetted by shortening the aspheric mirror (starting at z_{3MAX} and working toward z_{3MIN}), spherical aberration could clearly be reduced. In order to study the effect of intentional vignetting, a ray trace program was prepared to obtain the rms spot diameter in the focal plane as a function of off-axis angle for various choices of z_{3MAX}, starting with the original value $z_{3MAX} = 113.498$ inches and working down to $z_{3MAX} = 110.498$ inches. The latter value makes the coma-free mirror about one half of its original length, and thus would produce approximately 50% vignetting. The results of the vignetting ray trace program are summarized in Table X. The percentage of vignetting for each different aspheric mirror length for the case in which the off-axis angle is zero was calculated as the percentage of aspheric mirror length removed -- i.e.,

$$\% \text{ vignetting} = \frac{113.498 - z_{3MAX}}{5.87} \times 100. \qquad (12)$$

For cases in which the off-axis angle is not zero, rays striking a given radial zone of the hyperboloidal mirror do not all strike the aspheric mirror at the same z-coordinate. The percentage of vignetting for off-axis rays therefore can not be estimated reliably by use of Eq. (12); the actual percentage of vignetting would have to be obtained by counting the number of rays which miss the shortened aspheric mirror at each given off-axis angle, which was not done in the present program. However, all that is really needed is an estimate of the percentage of incident x-ray photon flux which

Table X. Spot diameter as a function of off-axis angle for various amounts of intentional vignetting created by shortening the coma-free aspheric third mirror.

OFF-AXIS ANGLE (arc-minutes)	z_{3MAX} (inches)	RMS SPOT DIAMETER (millimeters)	PERCENTAGE VIGNETTING
0.0	113.498	4.21*	0
	112.898	3.98	10.2
	112.298	3.52	20.4
	111.698	3.06	30.7
	111.098	2.60	40.9
	110.498	2.14	51.1
2.0	113.498	4.45*	
	112.898	4.31	
	112.298	3.92	
	111.698	3.52	
	111.098	3.14	
	110.498	2.79	
4.0	113.498	4.95*	
	112.898	4.93	
	112.298	4.82	
	111.698	4.59	
	111.098	4.34	
	110.498	4.13	
6.0	113.498	5.66*	
	112.898	5.70	
	112.298	5.77	
	111.698	5.83	
	111.098	5.77	
	110.498	5.66	

*The small discrepancies between the rms spot diameters for zero vignetting in this table and the corresponding rms spot diameters given in Table IX are due to the fact that the incident rays were entered slightly differently in the two programs.

is rejected by shortening the coma-free aspheric mirror. The on-axis vignetting data suffice for this purpose.

It is evident from Table X that spherical aberration can be significantly reduced if an appreciable amount of vignetting can be tolerated. If 51.1% vignetting were allowed, for example, the on-axis spot diameter could be reduced from 4.21 mm to 2.14 mm, which is a 49% decrease in spot size. The reduction in spot diameter at off-axis angles, however, is less dramatic. At 2.0 arc-minutes, for example, 51.1% vignetting yields only a 37% reduction in spot size, while at 4.0 arc-minutes the same amount of vignetting only produces a 17% reduction in spot size. At 6.0 arc-minutes, vignetting has virtually no effect on spot size.

Even though 51.1% vignetting cuts the on-axis spot size nearly in half, the spot is still too large to be well matched to an array of position-sensitive proportional counters. The performance of a spherical-aberration-free mirror placed immediately behind the S-056 mirror assembly is vastly superior to that of a vignetted coma-free mirror over the entire field of view. It would be interesting to study the performance of a coma-free mirror situated just behind the S-056 mirror assembly — or, for that matter, situated at a number of different locations along the optical axis. Unfortunately, time did not permit investigation of this topic under the present contract.

V. DUAL-CHANNEL OPERATION

As the final phase of the present study, a specific model of the TMXRT was designed with the aspheric third mirror moved as far forward as possible, and the characteristics of the composite image formed by simultaneous operation of both channels were studied. In this model of the TMXRT, the aspheric mirror was moved forward until its maximum radius was just equal to the minimum radius of the S-056 hyperboloidal mirror. Under these circumstances, the front edge of the aspheric mirror was 2.25 inches in front of the plane of the back of the S-056 hyperboloidal mirror. The situation is summarized in Fig. 12. In this arrangement, the average glancing angle of incidence on the aspheric third mirror is 0.99°, and the average focal length of the H-A channel is 76.3 inches, nearly equal to that of the P-H channel.

In order to study the properties of the composite image, separate ray traces were made of the P-H and the H-A channels to determine the rms spot diameter and the location of the center of the spot as a function of off-axis angle for each channel. The results are summarized in Table XI. It will be observed from Table XI that the rms spot diameter for the P-H channel is much smaller than that for the H-A channel at any given off-axis angle. At an off-axis angle of 1.0 arc-minute, the P-H channel spot diameter is only 1/52 of the H-A channel spot diameter. At 5.0 arc-minutes, this ratio has increased to approximately 1/20, while at 10.0 arc-minutes it is roughly 1/10. Since the focal lengths of the two channels are nearly equal, the distances from the optical axis to the centers of the spots formed by the two channels are nearly equal at any given off-axis angle. The two spots therefore blend reasonably well into a single composite image.

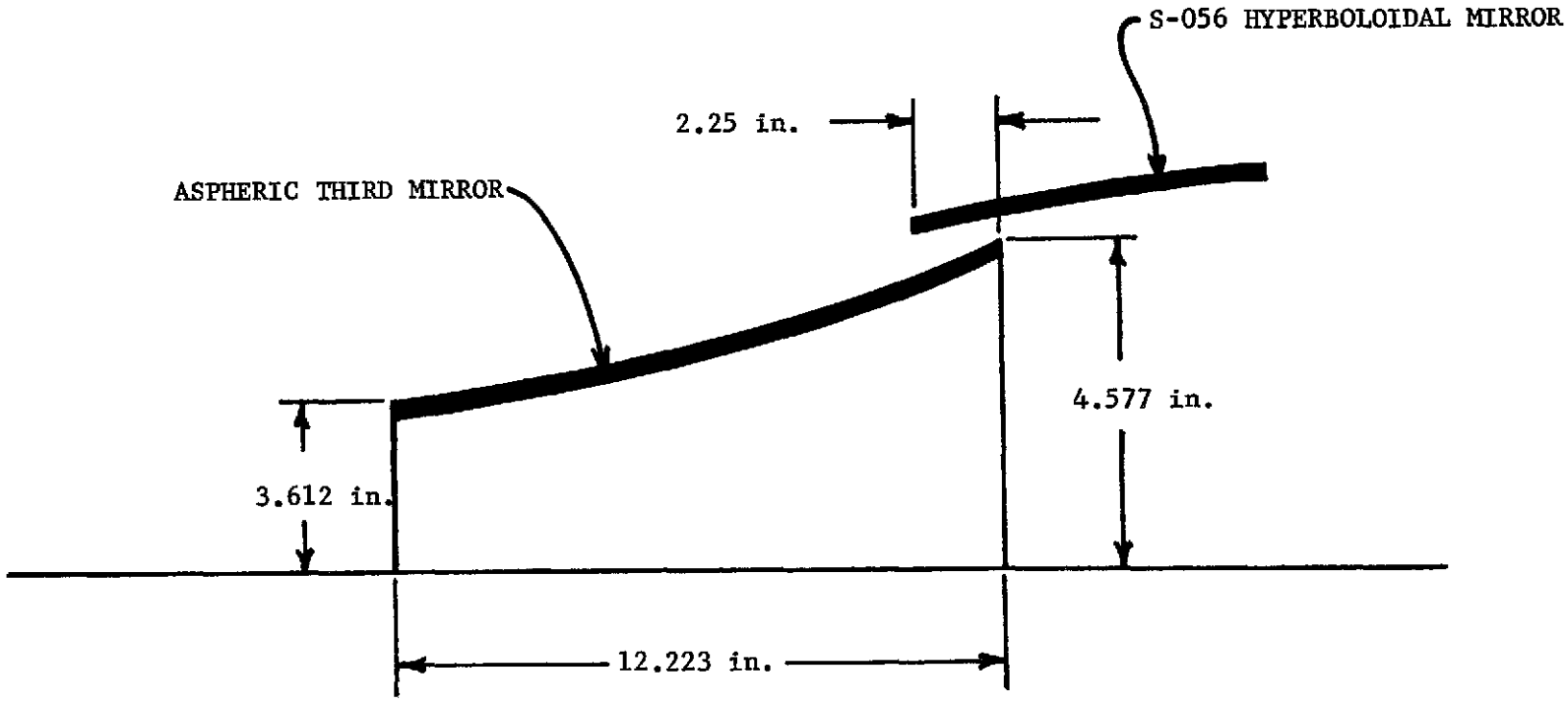

Figure 12. Size and placement of the aspheric third mirror used to study the dual-channel imaging characteristics of the TMXRT.

Table XI. Spot diameter and location of spot center for the P-H and H-A channels as a function of off-axis angle.

	P-H CHANNEL		H-A CHANNEL	
OFF-AXIS ANGLE (arc-minutes)	RMS SPOT DIAMETER (millimeters)	DISTANCE FROM OPTICAL AXIS TO SPOT CENTER (millimeters)	RMS SPOT DIAMETER (millimeters)	DISTANCE FROM OPTICAL AXIS TO SPOT CENTER (millimeters)
0.0	9.55×10^{-11}	0.00	9.70×10^{-6}	0.00
1.0	1.41×10^{-3}	0.55	7.30×10^{-2}	0.53
2.0	3.85×10^{-3}	1.11	0.15	1.06
3.0	7.67×10^{-3}	1.66	0.22	1.59
4.0	1.28×10^{-2}	2.22	0.29	2.12
5.0	1.94×10^{-2}	2.77	0.36	2.66
6.0	2.74×10^{-2}	3.33	0.42	3.19
7.0	3.67×10^{-2}	3.88	0.49	3.72
8.0	4.77×10^{-2}	4.44	0.57	4.25
9.0	5.98×10^{-2}	4.99	0.62	4.80
10.0	7.23×10^{-2}	5.55	0.69	5.33

Fig. 13, for example, summarizes the properties of the composite image in the focal plane at an off-axis angle of 5.0 arc-minutes.

The model of the TMXRT presented in this section operates quite satisfactorily. The spot formed by the P-H channel falls nicely within the boundaries of the larger spot formed by the H-A channel, and the rms spot diameter of the H-A channel is only 0.69 mm (1.2 arc-minutes) at an off-axis angle of 10.0 arc-minutes. The TMXRT has a total collecting area of 56.0 cm^2 (14.9 cm^2 from the paraboloidal mirror plus 41.1 cm^2 from the hyperboloidal mirror), or approximately 3.8 times the collecting area of the S-056 x-ray telescope (14.9 cm^2 from the paraboloidal mirror only). Dual-channel operation will only be feasible at soft x-ray wavelengths because of the relatively large glancing angle of incidence for rays which strike the hyperboloidal mirror directly (2.75°, nearly constant over the entire length of the hyperboloidal mirror).

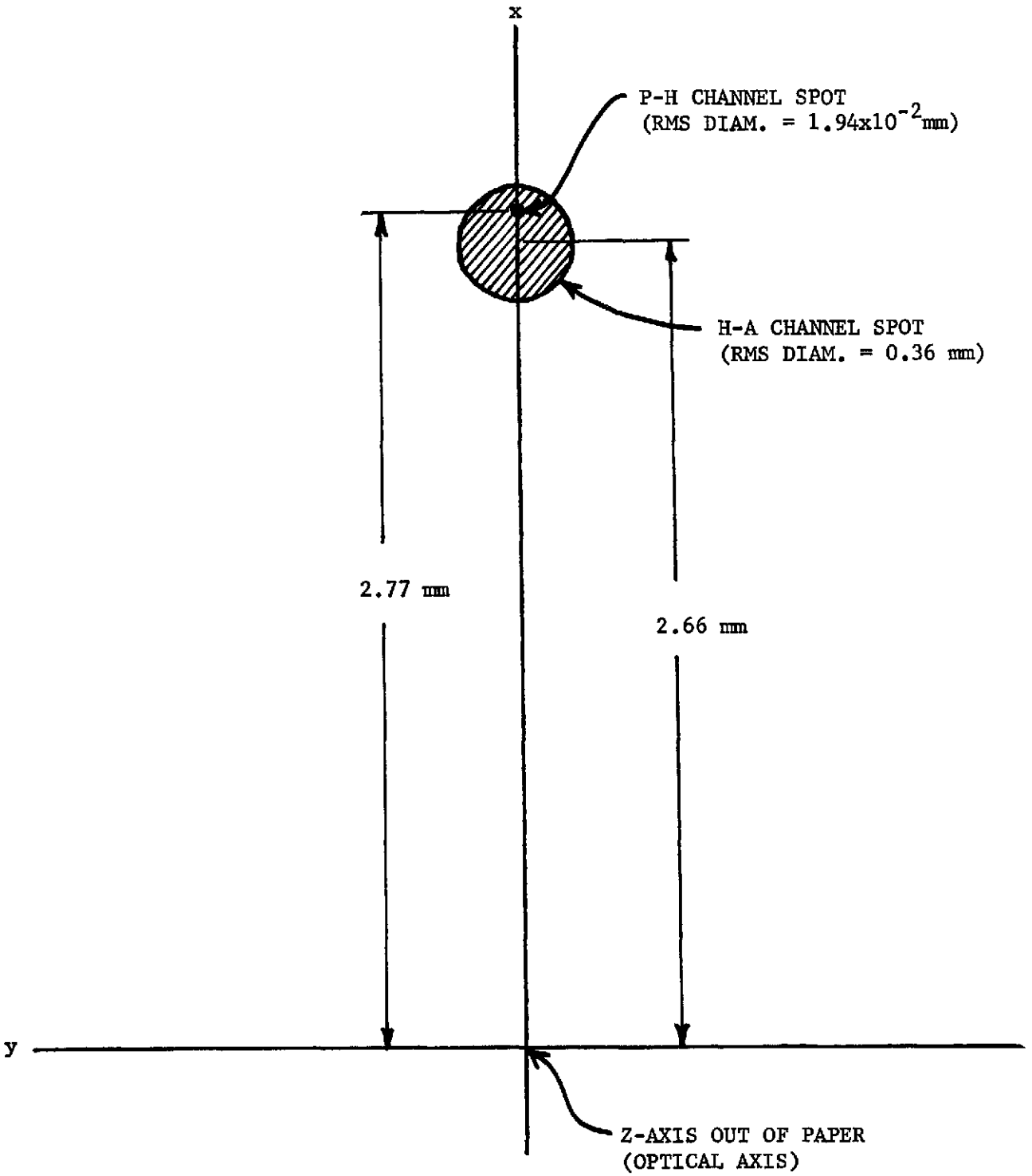

Figure 13. Composite image formed in the focal plane by simultaneous operation of both channels at an off-axis angle of 5.0 arc-minutes.

REFERENCES

1. J. W. Foreman, Jr. and J. M. Cardone, "Design and Mathematical Analysis of a Dual-Channel X-Ray Telescope Based on ATM S-056 X-Ray Telescope Hardware", Interim Progress Report, University of Montevallo, Montevallo, Alabama (August, 1972).

2. J. W. Foreman, Jr., et al., "Analytical Study of the Imaging Characteristics of the Goddard ATM X-Ray Telescope", Report No. SP-505-0279, Space Support Division, Sperry Rand Corporation, Huntsville, Alabama (September, 1969), Appendix A.

3. See, for example, H. P. Brueggemann, Conic Mirrors, Focal Press, New York (1968), pp. 84-86. Brueggemann discusses the use of path length equalization to eliminate spherical aberration as it was originally employed by Schwarzschild in designing the forerunner of the modern Ritchey-Chretién telescope.

4. D. P. Feder, "Optical Calculations with Automatic Computing Machinery", J. Opt. Soc. Am. 41, 630 (1951).

5. See, for example, F. B. Hildebrand, Introduction to Numerical Analysis, McGraw-Hill Book Co., Inc., New York (1956), Chapter 7.

6. A. K. Rigler and T. P. Vogl, "Spline Functions: An Alternative Representation of Aspheric Surfaces", Appl. Optics 10, 1648 (1971)

7. Reference 2, pp. 14-26.

8. Reference 2, Appendix C.